Progress In Electromagnetics Research B, Vol. 34, 187–204, 2011

QUASI-STATIC COMPLEX IMAGE METHOD FOR A CURRENT POINT SOURCE IN HORIZONTALLY STRATIFIED MULTILAYERED EARTH

Z.-X. Li*, G.-F. Li, J.-B. Fan, and Y. Yin

Center of Parallel Computing, China Electrical Power Research Institute, No. 15, East Road of Xiaoying, Qinghe, Haidian, Beijing 100192, China

Abstract—Based on quasi-static electromagnetic field theory, recently grounding system under alternative currents (AC) substation has been studied with equal potential and unequal potential models. In these numerical models, the closed form of Green's function for a point source within a horizontal multilayered earth model and its quasi-static complex image method have been fully discussed. However, less information about how to achieve the closed form of Green's function through Matrix Pencil method is presented in these references. In this paper, we discuss how the kernel of the Green's function can be expanded into a finite exponential series.

1. INTRODUCTION

The grounding problems under AC substation have been studied based on either the electrostatic field theory or the direct current electric field theory, with the equal potential model [1–6] or unequal potential model [7, 8]. However, these models ignore the mutual capacitative interactions between leakage currents along pairs of short conductors. Mutual induction interactions between branch currents along a pair of short conductors have also been overlooked in the unequal potential model. Although the hypothesis for the electrostatic field theory can be accepted under 50 Hz or 60 Hz work frequency condition, restrictions for the model will be evident for more general cases. For example, if a large resistivity of earth is observed for a buried grounding grid, the imaginary number of grounding impedance will be large [9]. In this case, grounding resistance substituting for grounding impedance will

Received 3 June 2011, Accepted 26 August 2011, Scheduled 13 September 2011

* Corresponding author: Zhong Xin Li (zxli@fudan.edu.cn).

be inappropriate. In other words, electrostatic field theory or direct current electric field theory is inappropriate for this type of grounding problem, and a more updated electromagnetic theory is required.

To better describe the grounding problem in low frequency domain (50 or 60 Hz and higher harmonic wave), in recent years the quasi-static electric field theory has been utilized to combine with the equal potential model [10–14] and unequal potential model [9, 15–22]. In these models, only the propagation effect of electromagnetic wave is ignored. Meanwhile, if a point source is buried in the horizontal multilayered earth, the scalar electrical potential (SEP) of a scalar monopole or the vector magnetic potential (VMP) of a vector dipole is satisfied with scalar or vector Poisson equation. After solving the scalar or vector Poisson equation for the monopole or dipole, scalar or vector Green's function for the monopole or dipole can be obtained. The infinite integral for Bessel function of the first kind of order zero has appeared within these Green's functions formulae. The infinite integral can be transformed into finite exponential series by Matrix Pencil (MP) method [23]. In this way, closed form of scalar or vector Green's function of monopole or dipole can be achieved. Among these derivation procedures we also discuss how to achieve a finite exponential series with MP method, called quasi-static complex image method (QSCIM). It should be pointed out that references [5] and [24] have also given finite exponential series for scalar Green's function of a scalar monopole based on Prony's method and are called complex image method. Actually, the complex image method should be called static complex image method due to its electrostatic field theory.

In this paper, QSCIM has been fully discussed based on the MP method. First, the procedure for vector or scalar Green's function of vector dipole or scalar monopole buried in horizontal multilayered earth model is compendiously introduced. Then the process to achieve finite exponential series for the kernel of Green's function based on MP method is discussed. Finally, numerical results for the kernel of the closed form of Green's function are carefully studied and discussed.

2. THEORY OF QUASI-STATIC COMPLEX IMAGE METHOD

2.1. The Closed Form of Scalar or Vector Green's Function of Monopole or Dipole

For a point source (scalar monopole or vector dipole) buried in horizontal multilayered earth model, we consider that a low frequency (50 or 60 Hz and higher harmonic wave) electromagnetic field occurs around the AC substation. Meanwhile, the size of grounding system

under the AC substation is limited, so the electromagnetic waves' propagation effect can be ignored. Hence, quasi-static electrical field can be regarded as a better theory for this grounding problem. Further, in this case, the SEP φ of a scalar monopole satisfies the scalar Poisson equation, and VMP $\bar{A}$ of a vector dipole satisfies the vector Poisson equation. Here we suppose that the point source current is located at the origin of the co-ordinate system (Fig. 1). The horizontal N_s-layer earth model is considered.

$$\nabla^2 \varphi_{ij}(x,y,z) = -\frac{\delta(z,y,z)\delta(ij)}{\overline{\sigma_i}} \tag{1}$$

where $i,j = 1,\ldots,N_s$, $\delta(x,y,z)$ is Dirac delta function for scalar monopole, and $\delta(ij)$ is Kronecker's symbol.

$$\nabla^2 \bar{A}_{ij}(x,y,z) = -\frac{\hat{\delta}(x,y,z)\delta(ij)}{\overline{\sigma_i}} \tag{2}$$

where $\hat{\delta}(x,y,z)$ is Dirac delta function for vector dipole.

After solving the Poisson Eqs. (1) and (2), we can get scalar Green's function for monopole and vector Green's function for vector dipole. For more details about the derivation process refer to [12, 14, 20–22] for scalar Greens' function and [20–22] for vector Green's function. Here, we will simply give, as examples, the formula for scalar Green's function G_{φ}^{11} of monopole and vector Green's

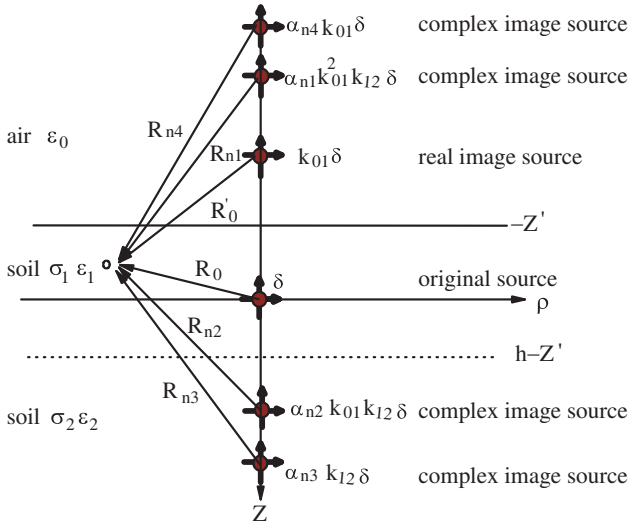

Figure 1. The point source current.

function G^{11}_{Azz} or G^{11}_{Axz} of dipole, both of which are buried in horizontal two-layer earth model with source and field point at the same layer.

For monopole case, from [12, 14, 20–22], we know

$$G^{11}_{\varphi}\left(k_\rho, z; k'_\rho, z'\right) = \frac{1}{4\pi\overline{\sigma_1}}\int_0^\infty \Big(e^{-k_\rho|z-z'|} - k^{\varphi}_{01}e^{-k_\rho(z+z')} + f^{\varphi}\left(k_\rho\right)\Big(k^{\varphi}_{01}k^{\varphi}_{12}e^{-k_\rho(2h_1+z+z')} + k^{\varphi}_{12}e^{-k_\rho(2h_1-z-z')} - k^{\varphi}_{01}k^{\varphi}_{12}e^{-k_\rho(2h_1+z-z')} - k^{\varphi}_{01}k^{\varphi}_{12}e^{-k_\rho(2h_1-z+z')}\Big)J_0(k_\rho\rho)dk_\rho \quad (3)$$

where $f^{\varphi}(k_\rho) = \frac{1}{(1+k^{\varphi}_{01}k^{\varphi}_{12}\cdot e^{-2k_\rho h_1})}$, $k^{\varphi}_{01} = \frac{\overline{\sigma_0}-\overline{\sigma_1}}{\overline{\sigma_0}+\overline{\sigma_1}}$, $k^{\varphi}_{12} = \frac{\overline{\sigma_1}-\overline{\sigma_2}}{\overline{\sigma_1}+\overline{\sigma_2}}$, $\overline{\sigma_0} = j\omega\varepsilon_0$, $\overline{\sigma_1} = \sigma_1 + j\omega\varepsilon_1$, $\overline{\sigma_2} = \sigma_2 + j\omega\varepsilon_2$, h_1 is thickness of the first layer earth. And $\rho = \sqrt{(x-x')^2+(y-y')^2}$

The kernel $f^{\varphi}(k_\rho)$ of scalar Green's function G^{11}_{φ} can be expanded into finite exponential series by the MP method,

$$f^{\varphi}(k_\rho) = \sum_{i=1}^{M}\alpha_i e^{\beta_i k_\rho} \quad (4)$$

Replacing $f^{\varphi}(k_\rho)$ of G^{11}_{φ} with the finite exponential series and employing the Lipschitz integration [20], we have

$$G^{11}_{\varphi}\left(x,y,z;x',y',z'\right) = \frac{1}{4\pi\overline{\sigma_1}}\left(\frac{1}{R} - \frac{k^{\varphi}_{01}}{R'} + \sum_{i=1}^{M}\alpha_i\left(\frac{\left(k^{\varphi}_{01}\right)^2 k^{\varphi}_{12}}{R_{i1}} + \frac{k^{\varphi}_{12}}{R_{i2}} - \frac{k^{\varphi}_{01}k^{\varphi}_{12}}{R_{i3}} - \frac{k^{\varphi}_{01}k^{\varphi}_{12}}{R_{i4}}\right)\right) \quad (5)$$

where $R=\sqrt{(x-x')^2+(y-y')^2+(z-z')^2}$, $R'=\sqrt{(x-x')^2+(y-y')^2+(z+z')^2}$, $R_{i(1-4)} = \sqrt{(x-x')^2+(y-y')^2+(\mathrm{sign}_a z + \mathrm{sign}_b z' + z_i)^2}$, in which $\mathrm{sign}_a = 1$ for R_{i1} and R_{i3}, $\mathrm{sign}_b = 1$ for R_{i3} and R_{i4}, $\mathrm{sign}_a = \mathrm{sign}_b = -1$ for others, $z_i = 2h - \beta_i$.

For vertical dipole case, from [20–22], we know

$$G^{11}_{Azz}\left(k_\rho, z; k'_\rho, z'\right) = \frac{\mu}{4\pi}\int_0^\infty \Big(e^{-k_\rho|z-z'|} - k^{TM}_{01}e^{-k_\rho(z+z')} + f^{TM}(k_\rho)\Big(k^{2TM}_{01}k^{TM}_{12}e^{-k_\rho(2h_1+z+z')} + k^{TM}_{12}e^{-k_\rho(2h_1-z-z')} - k^{TM}_{01}k^{TM}_{12}e^{-k_\rho(2h_1+z-z')} - k^{TM}_{01}k^{TM}_{12}e^{-k_\rho(2h_1-z+z')}\Big)J_0(k_\rho\rho)dk_\rho \quad (6)$$

where $f^{TM}(k_\rho) = \frac{1}{(1+k^{TM}_{01}k^{TM}_{12}\cdot e^{-2k_\rho h_1})}$, $k^{TM}_{01} = \frac{\overline{\sigma_1}-\overline{\sigma_0}}{\overline{\sigma_1}+\overline{\sigma_0}}$, $k^{TM}_{12} = \frac{\overline{\sigma_2}-\overline{\sigma_1}}{\overline{\sigma_2}+\overline{\sigma_1}}$.

Since we know $k^{TM}_{01} = -k^{\varphi}_{01}$ and $k^{TM}_{12} = -k^{\varphi}_{12}$, and we can observe that the kernel $f^{\varphi}(k_\rho)$ and $f^{TM}(k_\rho)$ are equal, it implies

$f^{TM}(k_\rho) = f^{\varphi}(k_\rho)$ except for $k_{ij}^{TM}(k_\rho) = -k_{ij}^{\varphi}(k_\rho)$, $(i, j = 1, \ldots, N_s)$. Similar to scalar Green's function G_{φ}^{11}, we have

$$G_{Azz}^{11}\left(x, y, z; x', y', z'\right) = \frac{\mu}{4\pi}\left(\frac{1}{R} - \frac{k_{01}^{TM}}{R'} + \sum_{i=1}^{M}\alpha_i\left(\frac{k_{01}^{2TM}k_{12}^{TM}}{R_{i1}} + \frac{k_{12}^{TM}}{R_{i2}} - \frac{k_{01}^{TM}k_{12}^{TM}}{R_{i3}} - \frac{k_{01}^{TM}k_{12}^{TM}}{R_{i4}}\right)\right) \quad (7)$$

where R, R', $R_{i(1-4)}$ are the same as those in scalar Green's function G_{φ}^{11} in Eq. (5).

For horizontal dipole case, from [20–22], we know

$$G_{Axz}^{11}\left(k_\rho, z; k'_\rho, z'\right) = \frac{\mu}{4\pi}\frac{\partial}{\partial x}\int_0^\infty \left(-k_{01}^{TM}e^{-k_\rho(z+z')} + f^{TM}(k_\rho)\left(k_{01}^{2TM}k_{12}^{TM}e^{-k_\rho(2h_1+z+z')} + k_{12}^{TM}e^{-k_\rho(2h_1-z-z')} - k_{01}^{TM}k_{12}^{TM}e^{-k_\rho(2h_1+z-z')} - k_{01}^{TM}k_{12}^{TM}e^{-k_\rho(2h_1-z+z')}\right)J_0(k_\rho\rho)\frac{dk_\rho}{k_\rho} \quad (8)$$

Just as in Green's function G_{Azz}^{11}, considering the Lipschitz integration's varied form [20], we have

$$G_{Axz}^{11}(x, y, z; x', y', z') = \frac{\mu}{4\pi}\frac{\partial}{\partial x}\left(-k_{01}^{TM}\ln\left(z' + R'\right) + \sum_{i=1}^{M}\alpha_i\left(k_{01}^{2TM}k_{12}^{TM}\ln\left(z_{i1}+R_{i1}\right) + k_{12}^{TM}\ln\left(z_{i2}+R_{i2}\right) - k_{01}^{TM}k_{12}^{TM}\ln\left(z_{i3} + R_{i3}\right) - k_{01}^{TM}k_{12}^{TM}\ln\left(z_{i4} + R_{i4}\right)\right)\right) \quad (9)$$

where R', $R_{i(1-4)}$ are the same as those in scalar Green's function G_{φ}^{11} in Eq. (5). Other parameters are $z' = z + z'$, $z_{i(1-4)} = \mathrm{sign}_a z + \mathrm{sign}_b z' + z_i$, in which $\mathrm{sign}_a = 1$ for z_{i1} and z_{i3}, $\mathrm{sign}_b = 1$ for z_{i3} and z_{i4}, $\mathrm{sign}_a = \mathrm{sign}_b = -1$ for others, $z_i = 2h - \beta_i$.

If a dipole was lying in general orientation, the dipole can be divided into horizontal and vertical dipole components.

The Green's function of horizontal dipole $G_{Axx}^{11} = \frac{\mu}{4\pi}\frac{1}{R}$ will not be discussed since it is a simple formula.

As we observe the kernels of Green's functions for both vertical or horizontal dipole and monopole, we see $f^{TM}(k_\rho) = f^{\varphi}(k_\rho)$. So for horizontal two layer earth model, only kernel $f(k_\rho)$ can be considered as the unified kernel formula to be expanded into finite exponential

series. This conclusion can apply to the Green function of all other vector dipoles or scalar monopoles buried in horizontal two-layer earth model with different field point locations, such as G_{φ}^{10}, G_{Azz}^{10}, G_{Axz}^{10}, G_{φ}^{12}, G_{Azz}^{12}, G_{Axz}^{12}, G_{φ}^{21}, G_{Azz}^{21}, G_{Axz}^{21}, G_{φ}^{22}, G_{Azz}^{22}, G_{Axz}^{22}, etc. Further, the same conclusion can be arrived at with vector or scalar Green's function of vector dipole or scalar monopole buried in other horizontal multilayered earth models, such as 3-layer or 4-layer earth model cases.

The kernel of closed form of Green's function for both scalar monopole and vector dipole buried in horizontal three-layer and four-layer earth model will be introduced next.

2.1.1. 3-layer Earth Model Case

$$f^A(k_\rho) = \frac{1}{f_1^A(k_\rho) + f_2^A(k_\rho)} \tag{10}$$

and

$$f_1^A(k_\rho) = 1 + k_{01}^A k_{12}^A e^{-2k_\rho h_1} + k_{12}^A k_{23}^A e^{-2k_\rho h_2} \tag{11}$$

$$f_2^A(k_\rho) = k_{01}^A k_{23}^A e^{-2k_\rho(h_1+h_2)} \tag{12}$$

where $A = TM$ for vector dipole case and $A = \varphi$ for scalar monopole case; $k_{23}^{\varphi} = \frac{\overline{\sigma_2}-\overline{\sigma_3}}{\overline{\sigma_2}+\overline{\sigma_3}}$, $\overline{\sigma_3} = \sigma_3 + j\omega\varepsilon_3$, $k_{23}^{TM} = -k_{23}^{\varphi}$, h_2 is the thickness of second layer earth.

2.1.2. 4-layer Earth Model Case

$$f^A(k_\rho) = \frac{1}{f_1^A(k_\rho) + f_2^A(k_\rho) + f_3^A(k_\rho) + f_4^A(k_\rho)} \tag{13}$$

and

$$f_1^A(x) = 1 + k_{01}^A k_{12}^A e^{-2k_\rho h_1} + k_{12}^A k_{23}^A e^{-2k_\rho h_2} \tag{14}$$

$$f_2^A(x) = k_{23}^A k_{34}^A e^{-2k_\rho h_3} + k_{01}^A k_{23} e^{-2k_\rho(h_1+h_2)} \tag{15}$$

$$f_3^A(x) = k_{12}^A k_{34}^A e^{-2k_\rho(h_2+h_3)} + k_{01}^A k_{12}^A k_{23}^A k_{34} e^{-2k_\rho(h_1+h_3)} \tag{16}$$

$$f_4^A(x) = k_{01}^A k_{34}^A e^{-2k_\rho(h_1+h_2+h_3)} \tag{17}$$

where $A = TM$ for vector dipole case and $A = \varphi$ for scalar monopole case; $k_{34}^{\varphi} = \frac{\overline{\sigma_3}-\overline{\sigma_4}}{\overline{\sigma_3}+\overline{\sigma_4}}$, $\overline{\sigma_4} = \sigma_4 + j\omega\varepsilon_4$, $k_{34}^{TM} = -k_{34}^{\varphi}$, h_3 is the thickness of third layer earth.

For simplified description of MP in this paper, only scalar monopole case is discussed below, which means that $f(k_\rho)$ is used to represent $f^{\varphi}(k_\rho)$.

2.2. Application range for the QSCIM

The maximum frequency of applicability of the method is limited by the quasi-stationary approximation of the electromagnetic fields, which means that the propagation effect of the electromagnetic field around the dipole can be neglected, so

$$e^{-jk_iR} \approx 1 \tag{18}$$

where $k_i^2 = j\omega\sqrt{\mu(\varepsilon_i + \frac{\sigma_i}{j\omega})}$, $i = 1, \ldots, N_s$.

2.3. MP Method

A function $f(x)$ can be expanded into finite exponential series, as below,

$$f(x) = \sum_{i=1}^{M} \alpha_i e^{\beta_i x} \tag{19}$$

The three parameters to be decided are M, α_i and β_i.

To get these parameters, we first decide the maximum sample points according to the characteristic of function $f(x)$, and the maximum value for $x_{\max}$ can thus be obtained according to the minimum $f(k_\rho)$ decided by set truncation precise. Once $x_{\max}$ is known, we can get uniformly discrete values of $f(x)$ within scope $(0 \le x \le x_{\max})$. Therefore, we have uniform discrete function values of $f(x)$ with $(f(0), f(1), f(2), \ldots, f(N))$ corresponding to the value of x as $(0, x_1, x_2, \ldots, x_{\max})$ or $(0, \triangle x, \ldots, i\triangle x, \ldots, (N-1)\triangle x)$. Here $\triangle x$ is the rate of sampling. We can obtain

$$f(x) \approx \sum_{i=1}^{M} \alpha_i z_i^k \quad (k = 0, \ldots, N-1) \tag{20}$$

here

$$z_i^k = e^{\beta_i \triangle x} \quad (i = 1, \ldots, M) \tag{21}$$

2.3.1. Method to Decide Number of M

Since we have total N number of uniform discrete function values of $f(x)$, we can get the matrix $[Y]$ from the sampling data $f(x)$ by combining $[Y_1]$ and $[Y_2]$ as

$$[Y] = \begin{bmatrix} f(0) & f(1) & \ldots & f(L) \\ f(1) & f(2) & \ldots & f(L+1) \\ \vdots & \vdots & & \vdots \\ f(N-L-1) & f(N-L) & \ldots & f(N-1) \end{bmatrix}_{(N-L)\times(L+1)}, \tag{22}$$

$$[Y_1] = \begin{bmatrix} f(0) & f(1) & \dots & f(L-1) \\ f(1) & f(2) & \dots & f(L) \\ \vdots & \vdots & & \vdots \\ f(N-L-1) & f(N-L) & \dots & f(N-2) \end{bmatrix}_{(N-L)\times L}, \quad (23)$$

$$[Y_2] = \begin{bmatrix} f(1) & f(2) & \dots & f(L) \\ f(2) & f(3) & \dots & f(L+1) \\ \vdots & \vdots & & \vdots \\ f(N-L) & f(N-L+1) & \dots & f(N-1) \end{bmatrix}_{(N-L)\times L}, \quad (24)$$

where L is referred as the pencil parameter [25].

Note that $[Y_1]$ is obtained from $[Y]$ by omitting the last column, and $[Y_2]$ is obtained from $[Y]$ by omitting the first column. The parameter L can be chosen between $N/3$ and $N/2$.

Next, a singular-value decomposition (SVD) of the matrix $[Y]$ can be implemented as

$$[Y] = [U][\Sigma][V]^H, \quad (25)$$

here, $[U]$ and $[V]$ are unitary matrices, composed of the eigenvectors of $[Y][Y]^H$ and $[Y]^H[Y]$, respectively, and $[\Sigma]$ is a diagonal matrix including the singular values of $[Y]$, i.e.,

$$[U]^H[Y][V] = [\Sigma], \quad (26)$$

The choice of the parameter M can be achieved at this stage by studying the ratios of various singular values to the largest one. Typically, the singular values beyond M are set equal to zero. The way which M is chosen is as follows. Observe the singular value σ_c such that

$$\frac{\sigma_c}{\sigma_{\max}} \approx 10^{-p}, \quad (27)$$

where p is the number of significant decimal digits in the data. For example, if the sampling data is accurate up to three significant digits, the singular values for which the ratio in Eq. (27) is below 10^{-3} are essentially useless and should not be used in the reconstruction of the sampling data.

We next introduce the "filtered" matrix, $[V']$, constructed so that it contains only M predominant right-singular vectors of $[V]$;

$$[V'] = [v_1, v_2, \dots, v_M], \quad (28)$$

The right-singular vectors from $M+1$ to L, corresponding to the small singular values, are omitted. Therefore,

$$[Y_1] = [U][\Sigma'][V_1']^H, \quad (29)$$

$$[Y_2] = [U][\Sigma'][V_2']^H, \tag{30}$$

where $[V_1']$ is obtained from $[V']$ with the last row of $[V']$ omitted; $[V_2']$ is obtained by deleting the first row of $[V']$; $[\Sigma']$ is obtained from the M columns of $[\Sigma]$ corresponding to the M predominant singular values.

2.3.2. Method to Decide β_i

To introduce the MP method, we can use two $(N-L)\times L$ matrices, Y_1 and Y_2. We can rewrite

$$[Y_2] = [Z_1][R][Z_0][Z_2], \tag{31}$$

$$[Y_1] = [Z_1][R][Z_2], \tag{32}$$

where

$$[Z_1] = \begin{bmatrix} 1 & 1 & \dots & 1 \\ z_1 & z_2 & \dots & z_M \\ \vdots & \vdots & & \vdots \\ z_1^{N-L-1} & z_2^{N-L-1} & \dots & z_M^{N-L-1} \end{bmatrix}_{(N-L)\times M}, \tag{33}$$

$$[Z_2] = \begin{bmatrix} 1 & z_1 & \dots & z_1^{L-1} \\ 1 & z_2 & \dots & z_2^{L-1} \\ \vdots & \vdots & & \vdots \\ 1 & z_M & \dots & z_M^{L-1} \end{bmatrix}_{M\times L}, \tag{34}$$

$$[Z_0] = \mathrm{diag}[z_1, z_2, \dots, z_M], \tag{35}$$

$$[R] = \mathrm{diag}[R_1, R_2, \dots, R_M], \tag{36}$$

where diag[•] represents a $M \times M$ diagonal matrix.

Now we introduce the matrix pencil

$$[Y_2] - \lambda[Y_1] = [Z_1][R]\{[Z_0] - \lambda[I]\}[Z_2], \tag{37}$$

where $[I]$ is the $M \times M$ identity matrix. We can demonstrate that, in general, the rank of $\{[Y_2]-\lambda[Y_1]\}$ will be M, provided $M \le L \le N-M$. However, if $\lambda = z_i, i = 1, 2, \dots, M$, the ith row of $\{[Z_0] - \lambda[I]\}$ is zero, and the rank of this matrix is $M-1$. Hence, the parameters z_i may be found as generalized eigenvalues of the matrix pair $\{[Y_2]; [Y_1]\}$. Equivalently, the problem of solving for z_i can be transformed into an ordinary eigenvalue problem,

$$\Big\{[Y_1]^+[Y_2] - \lambda[I]\Big\}, \tag{38}$$

where $[Y_1]^+$ is Moore-Penrose pseudo-inverse of $[Y_1]$ and defined as

$$[Y_1]^+ = \left\{[Y_1]^H[Y_1]\right\}^{-1}[Y_1]^H, \tag{39}$$

where the superscript "H" denotes the conjugate transpose.

The eigenvalues of the matrix

$$\{[Y_2] - \lambda[Y_1]\}_{L\times M} \Longrightarrow \{[Y_1]^+[Y_2] - \lambda[I]\}_{M\times M} \tag{40}$$

are equivalent to the eigenvalues of the matrix

$$\left\{[V_2']^H - \lambda[V_1']^H\right\} \Longrightarrow \left\{[V_1']^H\right\}^+ \left\{[V_2']^H\right\}^+ - \lambda[I] \tag{41}$$

This methodology can be used to solve for z_i.

Lastly, we point out that in this case z_i represent β_i according to Eq. (21).

2.3.3. Method to Decide α_i

Once M and z_i are known, α_i are solved with the help of the following linear least-squares problem:

$$\begin{bmatrix} f(0) \\ f(1) \\ \vdots \\ f(N-1) \end{bmatrix} = \begin{bmatrix} 1 & 1 & \dots & 1 \\ z_1 & z_2 & \dots & z_M \\ \vdots & \vdots & & \vdots \\ z_1^{N-1} & z_2^{N-1} & \dots & z_M^{N-1} \end{bmatrix} \begin{bmatrix} \alpha_1 \\ \alpha_2 \\ \vdots \\ \alpha_M \end{bmatrix}, \tag{42}$$

3. SIMULATION RESULT ANALYSIS

3.1. Numerical Results for QSCIM

For two-layer earth model, we give conductivities 600^{-1} S/m, 30^{-1} S/m and permittivities $5\varepsilon_0$, $12\varepsilon_0$ to the first and second layers of the earth, respectively. The thickness of the first layer earth is 5 m, and frequency is 50 Hz. Applying the MP approach, the kernel of Green's function will arrive at relative error 0.1% with only three terms of quasi-static complex images. Figs. 2 and 3 show this monotone function and superposition situation of two curves from function and simulation for both the real and imaginary parts. The coefficients of quasi-static complex images are given in Table 1.

From Table 1, we know that there are a pair of conjugate complex numbers, α_n and $\beta_n\,(n = 2, 3)$, which occur in electrostatic field complex images [24]. Reference [24] explains that "It is to be pointed out that the complex images, in general, have complex locations and amplitudes. In electrostatics, the complex images come in conjugate

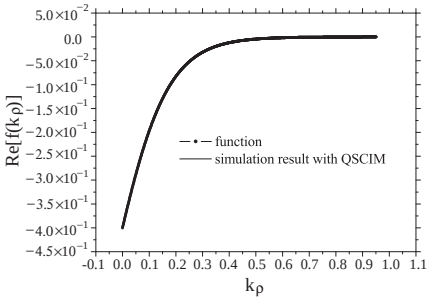

Figure 2. Two curves from function $f(k_\rho)$ and its simulation for 2-layer earth case (real part).

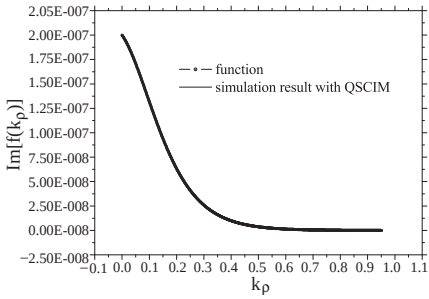

Figure 3. Two curves from $f(k_\rho)$ and its simulation for 2-layer earth case (imaginary part).

Table 1. Coefficients of quasi-static complex images for a two-layer earth model.

n	α_n	β_n
1	$0.646\angle - 4.328 \times 10.^{-5}$	$9.950\angle 7.227 \times 10.^{-7}$
2	$0.141\angle - 29.313$	$19.662\angle - 14.338$
3	$0.141\angle + 29.313$	$19.662\angle + 14.338$

pairs to give the real potential field value". Here, although quasi-static electrical field is chosen for the mathematical model, conjugate complex images also occur.

For the three-layer earth model, the earth's conductivities and permittivities are $\sigma_1 = 55.66^{-1}\,\mathrm{S/m}$, $\sigma_2 = 218.31^{-1}\,\mathrm{S/m}$, $\sigma_3 = 83.7^{-1}\,\mathrm{S/m}$, $\varepsilon_1 = 8\varepsilon_0$, $\varepsilon_2 = 12\varepsilon_0$ and $\varepsilon_3 = 6\varepsilon_0$, respectively. The first layer earth height is 3.867 m, and the secondary layer earth height is 3.432 m. With the MP approach, three terms of quasi-static complex images will arrive at relatively error 0.08%. From Figs. 4 and 5, we can see that the two curves are superposed. The three quasi-static complex images's coefficients are given in Table 2. From Table 2, we know that there is a pair of conjugate complex numbers, α_n and β_n ($n = 2, 3$).

For four-layer earth model, the earth's conductivities and permittivities are $\sigma_1 = 54.66^{-1}\,\mathrm{S/m}$, $\sigma_2 = 18.31^{-1}\,\mathrm{S/m}$, $\sigma_3 = 223.7^{-1}\,\mathrm{S/m}$, $\sigma_4 = 12.72^{-1}\,\mathrm{S/m}$, $\varepsilon_1 = 5\varepsilon_0$, $\varepsilon_2 = 12\varepsilon_0$, $\varepsilon_3 = 6.8\varepsilon_0$ and $\varepsilon_4 = 2.8\varepsilon_0$, respectively. The first layer earth height is 3.867 m, secondary layer earth height 3.432 m, and third layer earth height 19.12 m. With the MP approach, eight terms of quasi-static complex images will arrive at a relative error 0.03%. From Figs. 6 and 7, we can see that the two curves superpose each other. The coefficients of the six quasi-static complex images are given in Table 3.

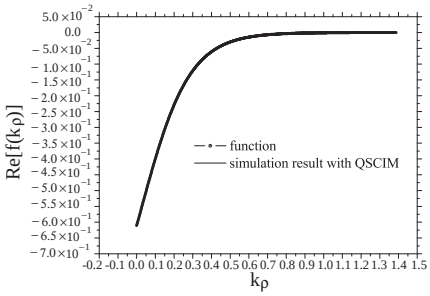

Figure 4. Two curves from $f(k_\rho)$ and its simulation for 3-layer earth case (real part).

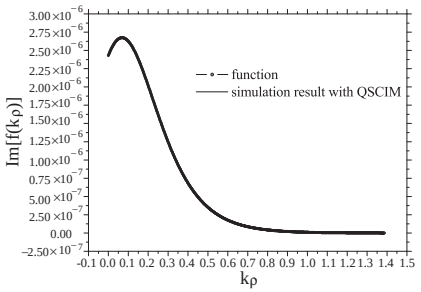

Figure 5. Two curves from $f(k_\rho)$ and its simulation for 3-layer earth case (imaginary part).

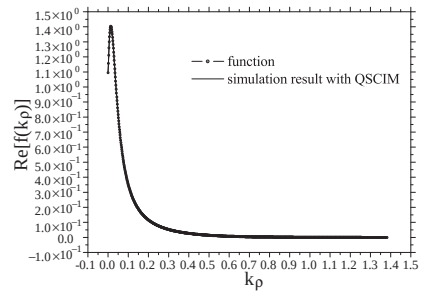

Figure 6. Two curves from $f(k_\rho)$ and its simulation for 4-layer earth case (real part).

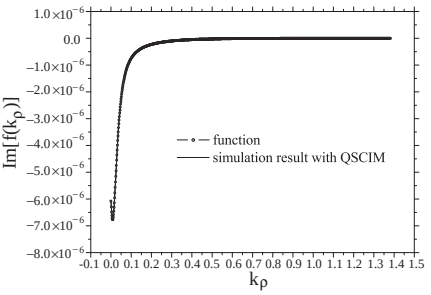

Figure 7. Two curves from $f(k_\rho)$ and its simulation for 4-layer earth case (imaginary part).

Table 2. Coefficients of quasi-static complex images for a three-layer earth model.

n	α_n	β_n
1	$1.093\angle - 4.933 \times 10^{-4}$	$7.208\angle 3.811 \times 10^{-5}$
2	$0.255\angle - 19.140$	$14.132\angle - 18.545$
3	$0.255\angle + 19.140$	$14.132\angle + 18.545$

From Table 3, we know that there are two pairs of conjugate complex images α_n and β_n ($n = 3, 4$ and $5, 6$).

3.2. Numerical Results for a Point Source

Once the closed form of vector and scalar Green's function of vector dipole and scalar monopole buried in horizontal multilayered earth model have been achieved, the numerical approximation of the electromagnetical field distribution generated by a harmonic current

Table 3. Coefficients of quasi-static complex images for a four-layer earth model.

n	α_n	β_n
1	$0.316\angle - 1.138 \times 10^{-4}$	$6.239\angle - 5.513 \times 10^{-6}$
2	$1.178\angle 8.152 \times 10^{-6}$	$19.118\angle 3.551 \times 10^{-5}$
3	$0.414\angle + 27.585$	$40.281\angle + 25.055$
4	$0.414\angle - 27.585$	$40.281\angle - 25.055$
5	$0.630\angle - 25.889$	$119.6802\angle - 27.482$
6	$0.630\angle + 25.889$	$119.6802\angle + 27.482$

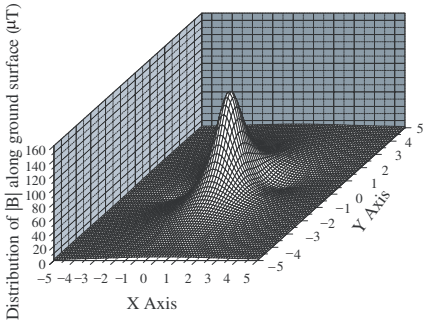

Figure 8. Distribution of $|B|$ along ground surface.

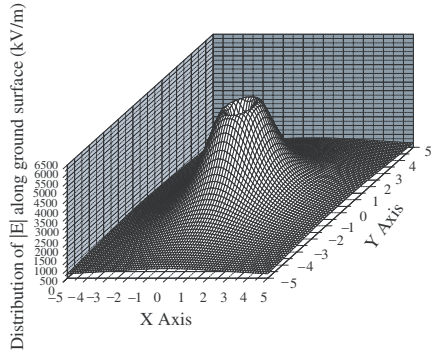

Figure 9. Distribution of $|E|$ along ground surface.

point source can be achieved. The source, in general, is located inside any layer of the horizontally multilayered earth. Meanwhile, a infinite series basing on Talyer's series, which approximate the electromagnetic field distribution in an observed layer has been reduced to a sufficiently large number of first members (usually not less than 10,000), which can be used as exact results for comparison.

To illustrate the high accuracy of the numerical procedure, a small subset of results from the treated numerical example will be given below. The point source is located in a four layer medium model, with the following parameters:

(i) Total number of layers of the earth model: $n = 4$.

(ii) Thickness of layers: $h_1 = 5\,\text{m}$, $h_2 = 12\,\text{m}$, $h_2 = 7\,\text{m}$.

(iii) The conductivities of the each layer of the earth model: $\sigma_1 = 100.0^{-1}\,\text{S/m}$, $\sigma_2 = 50.0^{-1}\,\text{S/m}$, $\sigma_3 = 900.0^{-1}\,\text{S/m}$ and $\sigma_4 = 200.0^{-1}\,\text{S/m}$.

Table 4. Module of SEP φ (V) and VMP A (wb/m).

or φ	Layer	Coordinates	QSCIM	Exact solution	Relative error (%)
φ	1	$(0,0,0)$	16523.85938	16523.03319	−0.0050
A_x	1	$(0,0,0)$	9.396927×10^{-5}	9.396476×10^{-5}	−0.0048
A_y	1	$(0,0,0)$	1.736482×10^{-5}	1.736407×10^{-5}	−0.0043
A_z	1	$(0,0,0)$	1.174063×10^{-6}	1.174023×10^{-6}	−0.0034
φ	1	$(50,0,1)$	535.11725	535.098521	−0.0035
A_x	1	$(50,0,1)$	1.879385×10^{-6}	1.879342×10^{-6}	−0.0023
A_y	1	$(50,0,1)$	3.472964×10^{-7}	3.472922×10^{-7}	−0.0012
A_z	1	$(50,0,1)$	1.236949×10^{-6}	1.236939×10^{-6}	−0.0008
φ	1	$(250,0,2)$	127.35694	127.35503	−0.0015
A_x	1	$(250,0,2)$	3.758741×10^{-7}	3.758640×10^{-7}	−0.0027
A_y	1	$(250,0,2)$	6.945872×10^{-8}	6.945796×10^{-8}	−0.0011
A_z	1	$(250,0,2)$	2.665560×10^{-7}	2.665541×10^{-7}	−0.0007
φ	2	$(0,0,5)$	2659.50391	2659.471996	−0.0012
A_x	2	$(0,0,5)$	2.349232×10^{-5}	2.349178×10^{-5}	−0.0023
A_y	2	$(0,0,5)$	4.341205×10^{-6}	4.341153×10^{-6}	−0.0012
A_z	2	$(0,0,5)$	4.978769×10^{-7}	4.975284×10^{-7}	−0.0007
φ	2	$(50,0,11)$	532.26379	531.78475	−0.0009
A_x	2	$(50,0,11)$	1.842889×10^{-6}	1.842876×10^{-6}	−0.0007
A_y	2	$(50,0,11)$	3.405521×10^{-7}	3.403478×10^{-7}	−0.0006
A_z	2	$(50,0,11)$	1.434278×10^{-6}	1.434271×10^{-6}	−0.0005
φ	2	$(250,0,12)$	127.28144	127.28042	−0.0008
A_x	2	$(250,0,12)$	3.755138×10^{-7}	3.755104×10^{-7}	−0.0009
A_y	2	$(250,0,12)$	6.939214×10^{-8}	6.939179×10^{-8}	−0.0005
A_z	2	$(250,0,12)$	3.560395×10^{-7}	3.560381×10^{-7}	−0.0004
φ	3	$(0,0,17)$	834.44586	834.44185	−0.00048
A_x	3	$(0,0,17)$	5.873079×10^{-6}	5.870436×10^{-6}	−0.00045
A_y	3	$(0,0,17)$	1.085301×10^{-6}	1.085299×10^{-6}	−0.00015
A_z	3	$(0,0,17)$	6.026217×10^{-8}	6.026210×10^{-8}	−0.00011
φ	3	$(50,0,20)$	428.53311	428.53225	−0.00020
A_x	3	$(50,0,20)$	1.756819×10^{-6}	1.756816×10^{-6}	−0.00015
A_y	3	$(50,0,20)$	3.246469×10^{-7}	3.246465×10^{-7}	−0.00011
A_z	3	$(50,0,20)$	1.177649×10^{-6}	1.177648×10^{-6}	−0.00009
φ	3	$(250,0,23)$	123.74226	123.74211	−0.00012

A_x	3	$(250, 0, 23)$	3.744301×10^{-7}	3.744296×10^{-7}	-0.00013
A_y	3	$(250, 0, 23)$	6.919188×10^{-8}	6.919180×10^{-8}	-0.00011
A_z	3	$(250, 0, 23)$	3.399787×10^{-7}	3.399785×10^{-7}	-0.00005
φ	4	$(0, 0, 24)$	663.63483	663.63231	-0.00038
A_x	4	$(0, 0, 24)$	4.085621×10^{-6}	4.085603×10^{-6}	-0.00044
A_y	4	$(0, 0, 24)$	7.549922×10^{-7}	7.549903×10^{-7}	-0.00025
A_z	4	$(0, 0, 24)$	3.392746×10^{-8}	3.392742×10^{-8}	-0.00012
φ	4	$(50, 0, 30)$	392.48398	392.48308	-0.00023
A_x	4	$(50, 0, 30)$	1.625727×10^{-6}	1.625723×10^{-6}	-0.00025
A_y	4	$(50, 0, 30)$	3.004222×10^{-7}	3.004218×10^{-7}	-0.00012
A_z	4	$(50, 0, 30)$	9.088801×10^{-7}	9.088797×10^{-7}	-0.00004
φ	4	$(250, 0, 33)$	122.54898	122.54871	-0.00022
A_x	4	$(250, 0, 33)$	3.728352×10^{-7}	3.728340×10^{-7}	-0.00033
A_y	4	$(250, 0, 33)$	6.889717×10^{-8}	6.889709×10^{-8}	-0.00012
A_z	4	$(250, 0, 33)$	3.252565×10^{-7}	3.252564×10^{-7}	-0.00002

(iv) The relative permitivities of each layer of the earth model: $\varepsilon_{r1} = 5.0$, $\varepsilon_{r2} = 25.0$ and $\varepsilon_{r3} = 50.0$ and $\varepsilon_{r4} = 30.0$.

(v) The location of the point source: $z = d = 1\,\text{m}$, so its coordinate $(0, 0, 1)$.

(vi) The point source current: (1000,0) A and 50 Hz for both scalar monopole point source and vector dipole point source.

(vii) The director of dipole point source: ($\theta_x = 20$, $\theta_y = 80$, $\theta_z = 72.863$).

The high accuracy of the numerical procedure based on a numerical approximation of the kernel functions is confirmed by results, which are presented in Table 4. The SEP and VMP values are computed at systematically chosen points in each of the four layers of earth. The computed relative error is found to be insignificant (Table 4). On the other hand, once SEP and VMP have been obtained for a point source, the electrical field intensity (EFI) E and magnetic field intensity (MEI) B of the point source can be calculated through the following formula.

$$\bar{B} = \nabla \times \bar{A} \tag{43}$$

$$\bar{E} = -j\omega\bar{A} - \frac{\partial\varphi}{\partial t}\hat{t} \tag{44}$$

Here $\hat{t}$ is unit director vector of the vector dipole.

Figs. 8 and 9 show the distribution of module of MFI $|B|$ and EFI $|E|$ along the surface of ground. From the two figures, apparently

different distributions between modulus of MEI B and EFI E can been seen.

4. SUMMARY

In this paper, the process how to achieve the closed form of Green's function for a point source (incudes monopole and dipole) within horizontal multilayered earth model by QSCIM has been fully discussed. First, the kernel of the closed form of Green's function for a point source buried in two to four layered horizontal earth model has been introduced. Then, we discuss how the kernel of the Green's function is to be expanded into finite exponential series by MP method. Lastly, the numerical results about QSCIM and electromagnetic field around a point source are discussed.

ACKNOWLEDGMENT

This work was supported by the China Electrical Power Research Institute.

REFERENCES

1. Sakis Meliopoulos, A. P., F. Xia, and G. J. Cokkinides, "An advanced computer model for grounding system analysis," *IEEE Transactions on Power Delivery*, Vol. 8, No. 1, 13–23, 1993.
2. Chow, Y. L., M. M. Elsherbiny, and M. M. A. Salama, "Surface voltages and resistance of grounding systems of grid and rods in two-layer earth by rapid Galerkin's moment method', *IEEE Transactions on Power Delivery*, Vol. 12, No. 1, 179–185, January 1997.
3. Vujevic, S., "Numerical analysis of potential distribution for a point current source in horizontally stratified multilayer earth," *Engineering Modelling*, Vol. 8, 21–29, 1995.
4. Vujevic, S. and M. Kurtovic, "Numerical analysis of earthing grids buried in horizontal stratified multilayer earth," *International Journal for Numerical Methods in Engineering*, Vol. 41, 1297–1319, 1998.
5. Zhang, L. P., J. S. Yuan, and Z. X. Li, "The complex image method and its application in numerical simulation of substation grounding grids," *Communication in Numerical Methods in Engineering*, Vol. 15, 835–839, 1999.

6. Colominas, I., F. Navarrina, and M. Casteleiro, "A numerical formula for grounding system analysis in stratified soils," *IEEE Transactions on Power Delivery*, Vol. 17, No. 2, 587–595, 2002
7. Yuan, J. S., H. N. Yang, L. P. Zhang, X. Cui, and X. S. Ma, "Simulation of substation grounding grids with unequal-potential," *IEEE Transactions on Magnetic*, Vol. 36, No. 4, 1468–1471, 2000.
8. Huang, L. and D. G. Kasten. "Model of ground grid and metallic conductor currents in high voltage a.c. substations for the computation of electromagnetic fields," *Electric Power Systems Research*, Vol. 59, 31–37, 2001.
9. Li, Z. X., G. F. Li, J. B. Fan, and C. X. Zhang "Numerical calculation of grounding system buried in vertical earth model in low frequency domain based on the boundary element method," *European Transactions on Electrical Power*, Vol. 19, No. 8, 1177–1190, 2009.
10. Rancic, P. D., L. V. Stefanovic, and D. R. Djordjevic, "A new model of the vertical ground rod in two-layer earth," *IEEE Transactions on Magnetic*, Vol. 28, No. 2, 1497–1500, 1992.
11. Rancic, P. D., L. V. Stefanovic, and D. R. Djordjevic, "An improved linear grounding system analysis in two-layer earth," *IEEE Transactions on Magnetic*, Vol. 32, No. 5, 5179–5187, 1996.
12. Li, Z. X., J. B. Fan, and W. J. Chen, "Numerical simulation of substation grounding grids buried in both horizontal and vertical multilayer earth model," *International Journal for Numerical Methods in Engineering*, Vol. 69, 2359–2380, 2007.
13. Vujevic, S. and P. Sarajcev, "Potential distribution for a harmonic current point source in horizontally stratified multilayer medium, *COMPEL: The International Journal for Computation and Mathematics in Electrical and Electronic Engineering*, Vol. 27, 624–637, 2008.
14. Li, Z. X., G. F. Li, and J. B. Fan, "Numerical simulation of substation grounding system in low-frequency domain based on the boundary element method with linear basis function," *Communication in Numerical Methods in Engineering*, Vol. 26, No. 12, 1819–1914, December 2010.
15. Sarajcev, P., S. Vujevic, and D. Lovric. "Time-harmonic current distribution on conductor grid in horizontally stratified multilayer medium," *Progress In Electromagnetics Research B*, Vol. 31, 67–87, 2011.
16. Otero, A. F., J. Cidras, and J. L. Alamo, "Frequency-dependent grounding system calculation by means of a conventional nodal

analysis technology," *IEEE Transactions on Power Delivery*, Vol. 14, No. 3, 873–877, July 1999.

17. Dawalibi, F., "Electromagnegtic fields generated by overhead and buried short conductors, Part 1 — Single conductor," *IEEE Transactions on Power Delivery*, Vol. 1, No. 4, 105–1111, 1986.
18. Dawalibi, F. and R. D. Southey, "Analysis of electrical interference from power lines to gas pipelines, Part 1 — Computational methods," *IEEE Transactions on Power Delivery*, Vol. 4, No. 3, 1840–1846, 1989.
19. Dawalibi, F., "Electromagnegtic fields generated by overhead and buried short conductors, Part 2 — Ground networks," *IEEE Transactions on Power Delivery*, Vol. 1, No. 4, 112–119, 1986.
20. Li, Z. X., W. J. Chen, J. B. Fan, and J. Y. Lu, "A novel mathematical modeling of grounding system buried in multilayer earth," *IEEE Transactions on Power Delivery*, Vol. 21, No. 3, 1267–1272, 2006.
21. Li, Z. X. and W. J. Chen, "Numerical simulation grounding system buried within horizontal multilayer earth in frequency domain," *Communication in Numerical Methods in Engineering*, Vol. 23, 11–17, 2007.
22. Li, Z. X. and J. B. Fan, "Numerical calculation of grounding system in low-frequency domain based on the boundary element method," *International Journal for Numerical Methods in Engineering*, Vol. 73, 685–705, 2008.
23. Sarkar, T. K. and O. Pereira, "Using the matrix pencil method to estimate the parameters of a sum of complex exponentials," *IEEE Antenna and Propagation Magazine*, Vol. 37, No. 1, 48–55, February 1995.
24. Chow, Y. L., J. J. Yang, and K. D. Srivastava, "Complex images of a ground electrode in layered soils," *Journal of Applied Physics*, Vol. 71, No. 2, 569–574, 1992.
25. Hua, Y. and T. K. Sarkar, "Generalized pencil-of-function method for extracting poles of an EM system from its transient response," *IEEE Transactions on Antenna and Propagation*, Vol. 37, No. 2, 229–234, February 1989.